PCCP

Using anion photoelectron spectroscopy of cluster models to gain insights into mechanisms of catalyst-mediated H_2 production from water

Journal:	*Physical Chemistry Chemical Physics*
Manuscript ID	CP-PER-09-2020-005055.R1
Article Type:	Perspective
Date Submitted by the Author:	27-Oct-2020
Complete List of Authors:	McMahon, Abbey; Indiana University, Chemistry Jarrold, Caroline; Indiana University, Chemistry

SCHOLARONE™
Manuscripts

Using anion photoelectron spectroscopy of cluster models to gain insights into mechanisms of catalyst-mediated H_2 production from water

Abbey J. McMahon and Caroline Chick Jarrold

Indiana University, Department of Chemistry, 800 E. Kirkwood Avenue, Bloomington, IN 47405

E-mail:cjarrold@indiana.edu

Abstract

Metal oxide cluster models of catalyst materials offer a powerful platform for probing the molecular-scale features and interactions that govern catalysis. This perspective gives an overview of studies implementing the combination of anion photoelectron (PE) spectroscopy and density functional theory calculations toward exploring cluster models of metal oxides and metal-oxide supported Pt that catalytically drive the hydrogen evolution reaction (HER) or the water-gas shift reaction. The utility in the combination of these experimental and computational techniques lies in our ability to unambiguously determine electronic and molecular structures, which can then connect to results of reactivity studies. In particular, we focus on the activity of oxygen vacancies modeled by *suboxide* clusters, the critical mechanistic step of forming proximal metal hydride and hydroxide groups as a prerequisite for H_2 production, and the structural features that lead to trapped dihydroxide groups. The pronounced asymmetric oxidation found in heterometallic group 6 oxides and near-neighbor group 5/group 6 results higher activity toward water, while group 7/group 6 oxides form very specific stoichiometries that suggest facile regeneration. Studies on the trans-periodic combination of cerium oxide and platinum as a model for ceria supported Pt atoms and nanoparticles reveal striking negative charge accumulation by Pt, which, combined with the ionic conductivity of ceria, suggests a mechanism for the exceptionally high activity of this system towards the water-gas shift reaction.

1 Introduction

It is difficult to overstate the importance of heterogeneous catalyst-driven reactions on daily life and the global economy, which provides ample motivation for exploring the molecular-scale details that govern catalysis. In particular, the production of molecular hydrogen from water decomposition, or the hydrogen evolution reaction (HER), is of enduring interest because of the advantage of using H_2 as a fuel. The "gold standard" catalyst for HER has been and continues to be platinum,[1–5] which is prohibitively expensive.

To a large extent, the exploitable activity from catalytic materials arises from defect sites- metal atoms in *non-traditional* oxidation states, or metal centers that are undercoordinated. Studies on single-atom catalysts deposited on surfaces are a poignant example of the local, non-bulk nature of a large portion of catalysis.[6–9] In practice, properties of catalyst materials are manipulated by complex processing, including reduction steps and nanoscale morphological preparations, which presents challenges with respect to reproducibility. In addition, dopant sites, binary and higher order oxides/sulfides, which offer potential of improved specificity and resilience, create highly-localized active sites.

Because catalyst-substrate interactions are local and molecular in scale, small clusters have been widely embraced as models for catalytically active sites,[10–67] but beyond their value as model systems, interesting molecular phenomena are probed in cluster studies, and theory is more tractable.

Over the past decade, our research program has explored the molecular-scale interactions between water and a range of cluster models to better characterize the molecular and electronic structural features of heterogeneous catalyst material defect sites that are active with respect to H_2 production from H_2O. In particular, we have focused on systems in which the metal centers are in lower-than-traditional oxidation states, or suboxides. Unlike stoichiometric clusters, metal-local orbitals are occupied in suboxides, which emulates charge localization in an oxygen vacancy in bulk metal oxides.[68] The tools we have used include anion photoelectron (PE) spectroscopy, experimental reactivity studies, and density functional theory (DFT) computational treatments of both electronic structure and reaction pathways. We have investigated

the chemical and physical properties of homo- and heteronuclear group 6 transition metal oxide clusters, near-neighbor transition metal oxides, cerium oxide clusters, and mixed platinum-cerium oxide clusters. These studies have elucidated several key electronic and molecular structure relationships to effective HER. The steps and barriers associated with the kinetics of weakly-bound $M_xO_z^-\cdot H_2O$ complex formation versus dissociative complex formation have been differentiated,[69] we have identified specific interactions that govern how water structurally couples to active sites, and found the importance of fluxionality of hydroxyl groups in H_2 release.[70] We have demonstrated how very modest differences in barrier heights affect whether trapped hydroxyl complexes or thermodynamically favored H_2 is formed.[71]

The combination of experimental and computational tools applied toward cluster models of catalysts has proven to be a powerful platform for studying these important processes. This focus of this perspective will be on the anion PE spectroscopic method, which, when combined with electronic structure calculations along with experimental and computational reactivity studies, provides a detailed picture of the electronic and molecular structures, which is essential for making the connection between structure and function.

2 Background

Determining cluster structures is motivated by the desire to connect molecular and electronic structures of catalytically active sites to their chemical and physical interactions with target molecules. In addition to anion PE spectroscopic characterization of cluster and cluster complex properties,[53−55,70−77] several examples of experimental approaches such as mass-analyzed threshold ionization (MATI),[78,79] photoionization efficiency spectroscopy,[80,81] UV/visible action spectroscopy,[11] vibrational predissociation spectroscopy,[12−19,21] photodissociation[82,83] collision induced dissociation (CID),[84−86] and ion reactivity studies[10,11,25,27,28,34−37,41,42,52,59,60,63,64,87,88] are included in the references. Collectively, these studies have contributed a wealth of knowledge on structures, bond energies, and photoactivity. Most of these studies involve ionic species because of their inherent mass selectability.

Cluster studies connect directly to defect sites on surfaces of bulk or nanoscale catalyst materials. However, a limitation of cluster studies in general is the absence of the attending surface and subsurface material, or the presence of solvents or additional gas molecules that may in some way influence catalyst activity. Studies on supported clusters,[89–91] single atom alloys[92,93] or solution phase homogeneous catalysts introduced to the gas phase by electrospray[94] address some of these limitations with the trade-off of losing gas-phase spectroscopic detail of molecular scale interaction. Beyond these surface studies, the area of nanoparticle catalysts warrants its own encyclopedic treatment.[95]

Within the wide range of gas-phase spectroscopic methods for modeling catalysis noted above, anion PE spectroscopy (combined with DFT calculations and reactivity studies) has particular value in the study of metals and metal oxides in providing a size-specific map of neutral electronic structures. Multiple close-lying spin states that are dark with respect to absorption can also be observed. Additionally, the method can provide information on molecular structures, and is sensitive to structure changes that accompany a change in local charge state, which is relevant for catalytic mechanisms involving charge transfer from the active site to the substrate. Following is a survey of the methods employed in our studies, as well as several systems we have explored.

3 Methods

3.1 Experimental

The experimental apparatus used in these studies has a pulsed laser-ablation style cluster source that can be coupled to a high-pressure fast flow reactor, a time-of-flight mass spectrometer for size-selection of cluster reactants and products, and a laser interaction region coupled to an electron kinetic energy analyzer for measuring the anion photoelectron spectra. The home-built apparatus has been described previously,[96,97] and only a very brief overview follows.

The surface of a target prepared by hydraulically compressing metal powder or, for heterometallic systems, combinations of metal powders, was laser ablated in a cluster source based on the Duncan and

Smalley design, which couples the target to a pulsed molecular beam valve and port for introducing the ablation laser.[98] Clusters coalesce and undergo collisional cooling in a high-pressure pulse of helium carrier gas in a 2.5-cm long, 3-mm diameter channel before expanding into a vacuum chamber and entering a time-of-flight mass spectrometer. Cluster-water reactivity studies, including several temperature-dependence and dual reactant studies, were conducted by injecting a variable number density of H_2O or other reactants into the clustering channel, and similarly mass analyzing via time-of-flight mass spectrometry.[99]

Mass selected clusters and their product anions were interrogated spectroscopically via fixed-frequency photoelectron spectroscopy. The output of a pulsed Nd:YAG laser is timed to intersect the anion of interest, and the kinetic energy distribution of the resulting photoelectrons is analyzed. This distribution is peaked due to transitions from the internally cold anions ($E_{internal}^{anion} \approx 0$) to discrete rovibronic levels of the neutral ($E_{internal}^{neutral}$, which has contributions from electronic, vibrational and rotational energy).

$$e^{-}KE = h\nu - EA - E_{internal}^{neutral} + E_{internal}^{anion}$$

The spectra are generally presented as electron counts as a function of electron binding energy, $e^{-}BE$, which reflects the relative energies of the initial anion state and final neutral states:

$$e^{-}BE = h\nu - e^{-}KE$$

And is independent of photon energy. Typically, one-electron transitions are the most prominent features in the spectrum, with an associated $\Delta s = \pm ½$ selection rule. The resolution of time-of-flight electron kinetic energy analyzer is not sufficient to resolve rotational spacings.

The undercoordinated metal oxides targeted in our studies feature metal centers that are more electron-rich than fully coordinated or oxidized clusters. The spectra therefore tend to be congested with multiple close-lying electronic transitions associated with nominally one-electron detachment of electrons from nearly degenerate *n*d or (*n*+1)s-like orbitals. One of the strengths of this spectroscopic method is its ability to map the low-lying electronic states of the neutral, some of which are dark with respect to direct absorption spectroscopy.

3.2 Computational

An essential element of making electronic and molecular structural assignments of the anion PE spectra of these cluster systems is an exhaustive computational survey of potential structures in a multitude of spin states. All calculations were carried out using the Gaussian (G03, G09, G16)[100−102] quantum chemistry software. In earlier studies ($W_xO_y^-$, $Mo_xO_y^-$ $Mo_{(3-x)}W_xO_y^-$, $MoVO_y^-$, $MoNbO_y^-$) geometry optimization calculations were performed with the unrestricted B3LYP hybrid density functional,[103−105] utilizing the Stuttgart–Dresden (SDD) relativistic pseudopotentials to replace all core electrons on the metals and an augmented version of the associated double-ζ basis set to treat the remaining metal valence electrons.[106] Diffuse *s*-, *p*-, and *d*-functions were included in the basis set to properly describe the increased radial extent of the anion wavefunction.[107] To allow for greater angular flexibility in optimizing the molecular orbitals, an additional polarization function (l + 1) was added to the basis sets of metals and oxygen atoms. To obtain triple-ζ quality basis sets for single point calculations, the aug-cc-pVTZ basis sets for oxygen and hydrogen atoms[108] and metal basis sets were augmented following the example of Martin and Sundermann.[109] Studies on the formation and stabilities of weakly $Mo_xO_y^-\cdot H_2O$ and $W_xO_y^-\cdot H_2O$ charge-dipole complexes the unrestricted M06 hybrid density functional method was utilized in place of B3LYP, as the latter functional has been shown to underestimate the energy of weakly bound complexes as well as barriers.[110]

For $Ce_xO_yH_z^-$ and $[CeO]Pt_n^-$ systems we again employed the unrestricted B3LYP hybrid density functional method paired with the Stuttgart relativistic, small core ECP28MWB_ANO pseudopotential with a 28 frozen electrons and an atomic natural orbital contracted Gaussian basis for the valence electrons for cerium.[111] For Pt, the frozen 60 electron ECP60MWB quasi-relativistic pseudopotential[106] with a valence basis set was used.[71] Oxygens and hydrogen we used the aug-cc-pVTZ Dunning correlation consistent basis set.[112]

Calculations on $Mn_xMoO_y^-$ cluseters utilized the def2-SVPP basis set.[113,114] The SDD effective core potentials were again employed to model the core electrons of the metals. To obtain accurate electronic

energies single-point calculations were performed on the optimized structures with the def2-TZVPP basis set.

Harmonic vibrational frequency calculations are performed on optimized structures to determine the nature of each stationary state found (no imaginary frequencies are accepted for minima, and only one imaginary frequency is accepted for transition states) and to evaluate the zero-point energies.

For a more detailed comparison between the calculated structures and the experimental spectra, simulated spectra were generated based on computationally predicted spectroscopic parameters, including adiabatic detachment energies (ADEs, the energy between the zero-point-corrected total energies of the anion and neutral), vibrational frequencies of the anions and neutrals, and normal coordinate displacements.[115] Home-written Labview codes input structures, vibrational frequencies and normal coordinates to calculate normal coordinate displacements and Franck-Condon factors, and generate a simulation with vibronic line positions and $e^{-}KE$-dependent linewidths. Vibrational "temperatures" can be adjusted independently for each active mode (though vibrational temperatures are typically set to 300K).

4 Group 6 transition metal oxide cluster anions and their reactions with water

Molybdenum and tungsten oxides have received considerable attention as potential electro- or photocatalysts for HER,[116-120] particularly in low-dimensional or meso- and nanoscale morphologies.[121−123] While Mo and W are both group 6 transition metals, there are several interesting distinctions between their respective oxides. WO_3, the strongly thermodynamically favored oxide, has a water-insoluble monoclinic, pseudo-cubic distorted structure, while MoO_3 has a water-soluble lamellar structure, and is more reducible than WO_3, with MoO_2 also being a fairly stable oxide. Cluster models of these species reflected bulk properties in several ways, as detailed below. In both the reactivity studies involving homo- and hetero-metal oxide clusters with water[69,99,124−128] and anion PE spectroscopic studies of the clusters and reaction products, the analysis of which was supported by extensive DFT studies, [70,71,129−138] the importance of Lewis

acid-base interactions, repulsion, barriers to hydroxide group fluxionality, and the relative stability of the Mo(IV) center govern the reactions.

To set the scene, the reactions observed were either cluster oxidation with H_2 release,

$$M_xO_y^- + H_2O \rightarrow M_xO_{y+1}^- + H_2 \qquad (1)$$

which generally occurs sequentially over a range of y values, or water addition, with no net change in oxidation state of the cluster:

$$M_xO_y^- + H_2O \rightarrow M_xO_{y+1}H_2^-. \qquad (2)$$

Water addition generally becomes more prevalent as the cluster approaches bulk oxidation ($y = 3x$), with several notable exceptions.

H_2 production in cluster- water reactions requires two conditions being satisfied: the hydrogens must have opposite charges, and they must be spatially proximal. Based on computational studies,[70,71,131] $M_xO_y^-$ + H_2O reactions initiate with local interactions involving alignment of the O−H bond on water along an M−O bond on the cluster. This interaction is guided by local dipole-dipole interactions and driven by the Lewis acidity of the metal center, followed by dihydroxide formation and subsequent rearrangement to proximal –H and –OH groups leading to H_2 production. Rearrangement is lower-barrier in suboxide systems, and clearly, the steric access to a Lewis acidic metal center plays a central role in the rate of initial complex formation.

Figure 1 shows the most stable structures of $Mo_2O_y^-$ and $W_2O_y^-$ (y = 4, 5) determined by a comparison between their respective PE spectra (blue traces) and M06/aug-cc-pvdz/SDD-based simulations (black traces).[71,125,132] We note here that a wide range of cluster structures were calculated (varying the number of bridge bonds between 0 and 3, symmetric versus asymmetric oxidation states of the two metal centers), and the structures that produced simulated spectra that were most consistent with the observed spectra coincided with the lowest energy isomers predicted for the anions. However, an important result that emerged from the electronic and molecular structure calculations is that the lowest energy neutral

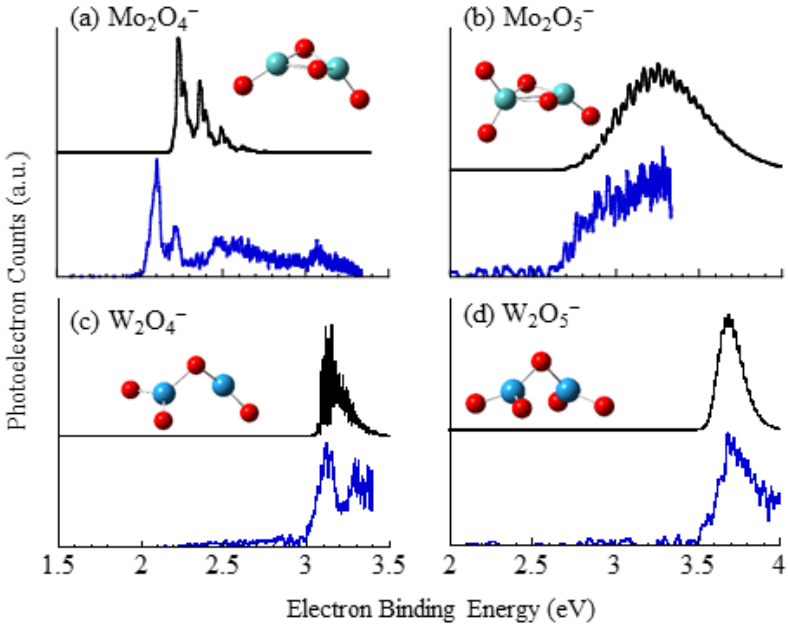

Figure 1. Anion PE spectra of (a) $Mo_2O_4^-$ (b) $Mo_2O_5^-$, (c) $W_2O_4^-$, and (d) $W_2O_5^-$ (blue traces) along with the structures with M06 computed spectroscopic parameters that produce the simulated spectra (black traces). These structures are also the lowest energy isomers computed for the clusters. (Red represents O-atoms, turquoise represents Mo atoms, blue represents W atoms). While Mo and W are group 6 transition metals, the Mo centers are bound by two bridge bonds, the W centers are bound by one.

structures are very frequently different from the lowest energy anions,[129–131] meaning that the detachment transition prepares a neutral in a metastable structure. When differences arise between the most stable structures of anions and neutrals, neutrals generally favor structures with more *M*–O–*M* bridge bonds than the anions. For example, the most stable neutral W_2O_4 and W_2O_5 structures are predicted to have two bridge bonds, and the observed transitions are from the lowest energy anions with a single bridge bond to a higher-lying neutral structure, resulting in higher transition energies. The broader implication is that charge-transfer from a catalytically active oxygen vacancy triggers a structural reorganization of O-atoms around the vacancy.

Both the $Mo_2O_4^-$ and $Mo_2O_5^-$ anions favor two bridge bonds, and their respective detachment transitions access the lowest energy neutral structures, with the associated lower transition energy. The spectra of the $W_2O_y^-$ anions show binding energies *ca.* 1 eV higher than their $Mo_2O_y^-$ congeners. Why are the $Mo_2O_y^-$ and $W_2O_y^-$ structures different? The $Mo_xO_y^-$ suboxide structures of the are governed by

maximizing the number of Mo centers in the +4 oxidation state (MoO_2 bulk is a metastable bulk oxidation state), while the $W_xO_y^-$ clusters do not affected by a relatively stable suboxide state.

With the structures of these clusters established, computational treatment of the reactivity studies could be conducted. An essential difference between the two group 6 transition metals is the barrier for –H and –OH rearrangement.[69] These barriers are generally submerged (below the free energy of the initial reactants) in $W_xO_y^-$ + H_2O reactions, while they are systematically, though modestly, higher in $Mo_xO_y^-$ + H_2O reactions, in some cases exceeding the internal energy gained in reactive complex formation. Therefore, $W_xO_y^-$ clusters generally undergo sequential oxidation to higher values of y than their $Mo_xO_y^-$ analogs. However, $Mo_xO_y^-$ clusters have higher reaction rate coefficients if $Mo_xO_{y+1}H_2^-$ formation is included. In addition to more favorable sterics for H_2O association with $Mo_xO_y^-$ clusters, the calculations predict that the Lewis acid-base ion-molecule complex is more strongly bound for $Mo_xO_y^-$ clusters than for $W_xO_y^-$ clusters. As a simple example, consider the different structures of $Mo_2O_5^-$ and $W_2O_5^-$ (Figure 1). The lowest energy structure of $Mo_2O_5^-$ provides a less hindered water addition site than the $W_2O_5^-$ ground state structure, and experimentally, $Mo_2O_5^-$ undergoes water addition more quickly than the analogous $W_2O_5^-$ + H_2O reaction. However, $Mo_2O_5^-$ exclusively forms $Mo_2O_6H_2^-$ in reactions with water, while $W_2O_5^-$ forms both the addition product and $W_2O_6^-$.

Again, interpretation and computational treatment of reactivity studies rely on the structures determined for these $M_2O_y^-$ clusters, which we extended to $M_3O_y^-$ (M = Mo, W; $y = 2 - 3x$) clusters, allowing us to explore the various modes of water addition, and finding that the most direct route for H_2 production involves two adjacent metal centers.[70] From the free energy pathways, a connection between the structural properties of these suboxide clusters with the propensity to either produce H_2 in reactions with water or to form metastable trapped species was found. In the case of the latter, we again turned to anion PE spectroscopy to determine that the trapped intermediates were dihydroxides rather than some other constitutional isomer. Figure 2 shows the PE spectra of both $Mo_3O_6^-$ (black trace) and $Mo_3O_6D_2^-$ generated by $Mo_3O_5^-$ + D_2O (blue traces) along with a simulation generated from the spectroscopic parameters

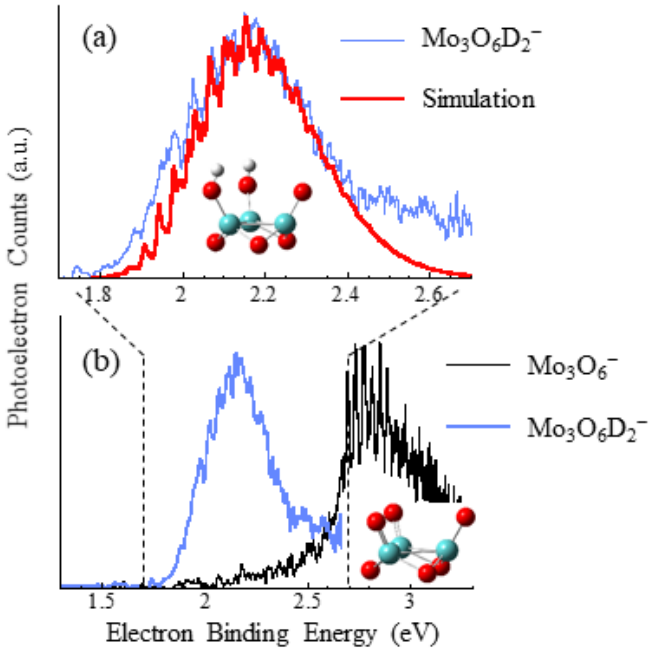

Figure 2. Anion PE spectrum of $Mo_3O_6D_2$ formed in the $Mo_3O_5^-$ + D_2O reaction [blue traces, panels (a) and (b)] along with (a) spectral simulation based on the B3LYP computed structure shown, and (b) in comparison with the PE spectrum of $Mo_3O_6^-$, which exhibits a similar vibrational progression but at a higher electron binding energy. Alternative structures in which one or both of the Mo-OD (or Mo-OH) groups are exchanged for one or two O-Mo-D (or O-Mo-H) hydride groups are predicted to have significantly higher electron binding energies and different Franck-Condon profiles. Turquoise represents Mo, red represents O, white represents H.

associated with the di-deuteroxide (dihydroxide, for the H_2O addition analog) structure shown in the top panel (red trace).[70] Alternative structures featuring one or two hydride (deuteride) groups rather than two hydroxide groups were predicted to be lower in energy, but also to have both higher ADE values as well as narrower Franck-Condon profiles. The spectrum is therefore an indication that a high-energy structure of $Mo_3O_6H_2^-$ is formed in the $Mo_3O_5^-$ + H_2O reaction. For all *kinetically* trapped water-addition products, the structure is a dihydroxide, and further calculations on the reaction free energy path predict relatively high barriers for rearrangement to a hydride-hydroxide structure necessary for H_2 production. We note here that in contrast to $Mo_3O_5^-$, $W_3O_5^-$ readily forms $W_3O_6^-$ + H_2 in reactions with water, with $W_3O_6H_2^-$ having modestly lower barriers to the necessary rearrangement, despite $W_3O_5^-$ and $Mo_3O_5^-$ having nearly identical structures.[70]

The results suggesting that $Mo_xO_y^-$ forms stronger Lewis acid-base complexes contradicts previous calculations on the Lewis acidity of stoichiometric group 6 (M_xO_{3x}, M = Cr, Mo, W) transition metal oxide clusters that align with the bulk periodic trend of increasing acidity with increasing row number.[139−141] We attributed the stronger interaction energies in $Mo_xO_y^-\cdot H_2O$ complexes to shorter Mo−O bond distances (smaller ionic radius of Mo) in *suboxides*. As new *M*–O bonds are formed in subsequent reactions leading toward bulk stoichiometry, W−O bonds become substantially stronger than Mo−O bonds, which is consistent with the stronger Lewis acidity of tungsten in +6 oxidation state. The bottom line is that reactive complex formation is faster for $Mo_xO_y^-$ clusters, but $W_xO_y^-$ reactions are more likely to lead to H_2 production.

The heterometallic $Mo_xW_xO_y^-$ clusters are a different story. The sequential oxidation of heterotrimetallic $Mo_xW_{3-x}O_y^-$ (x = 1, 2) clusters proceeded to higher values of y than both $Mo_3O_y^-$ and $W_3O_y^-$.[125] The anion PE spectra and calculations on $Mo_xW_{3-x}O_y^-$ and $MoWO_y^-$ heterometallic clusters were consistent with structures in which the Mo centers were consistently in a *lower* oxidation state than W until W was fully saturated, whereupon the Mo center would undergo oxidation.[134] As the most extreme example, $MoWO_3^-$ could be described as Mo^- atomic anion in an ion-dipole complex with neutral WO_3. Until the cluster is fully oxidized, the Mo center remains an electron-rich, sterically unhindered and relatively acidic locus for initial water complex formation. The disparate oxidation states in Mo-W mixed suboxide clusters reflects the higher oxophilicity of W (0.8 versus 0.6, based on the scale developed by Kepp),[142] which is born out in the greater reducibility of Mo.

To summarize the main findings, the $Mo_xO_y^- + H_2O \rightarrow Mo_xO_y^-\cdot H_2O$ electrostatic complex formation is more exothermic (and also proceeds with higher reaction rates) than the analogous $W_xO_y^-\cdot H_2O$ complex energies of formation, while $W_xO_y^-$ clusters are oxidized by water to higher values of y. Mo-W heterometallic oxide clusters, with the Mo center(s) in lower oxidation states than adjacent W center(s), are more reactive than both the homometallic homologs. For both the homo- and hetero-group 6 suboxide clusters, the most stable structures for the anions are frequently different than those for the neutral,

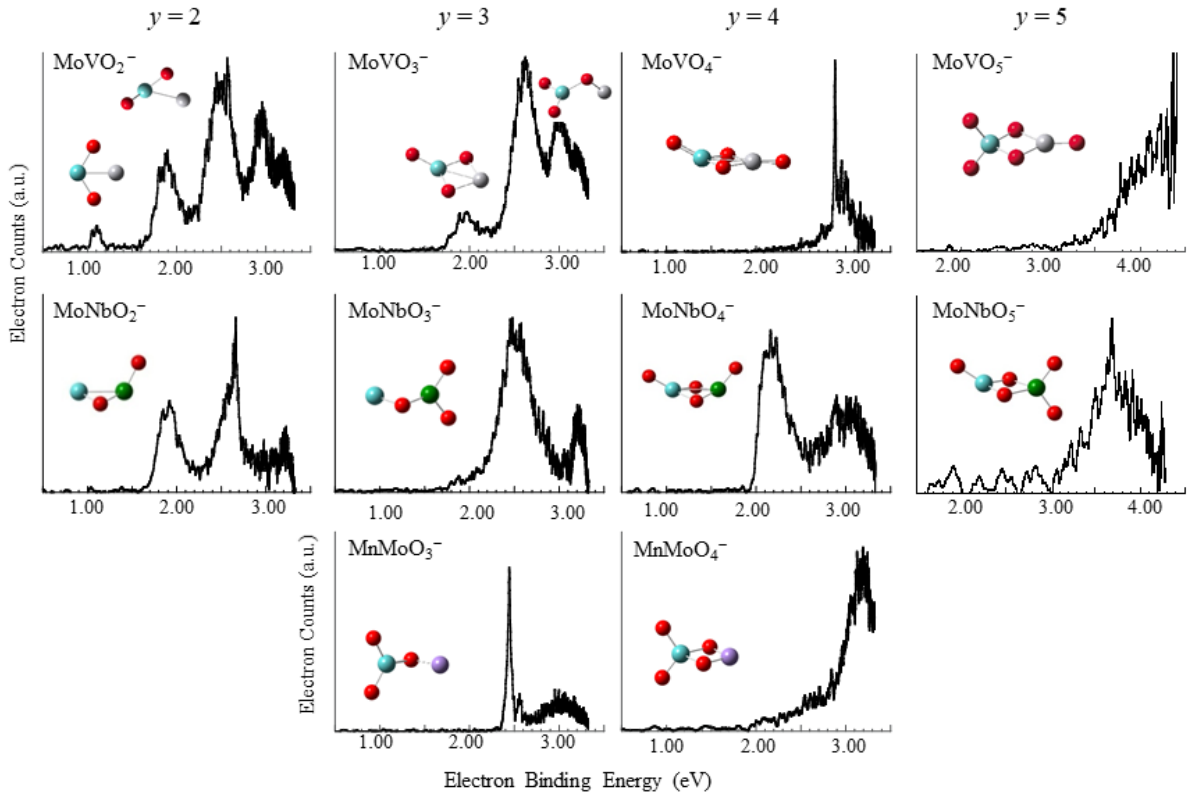

Figure 3. Anion PE spectra of near-neighbor hetero-transition metal oxides in a range of oxidation states, along with the computationally determined structures, showing generally higher Mo oxidation states in $MoVO_y^-$ clusters (top row), higher Nb oxidation states in $MoNbO_y^-$ (center row) and a narrower oxide distribution of $MnMoO_y^-$ reflecting the particular stability of Mn^{2+} combined with the stability of the +4 and +6 oxidation states of Mo. Turquoise represents Mo, red represents O, grey represents V, green represents Nb, rose represents Mn.

suggesting any charge-transfer from a negatively charged O-vacancy enter creates a structural change in which a terminal *M*=O bond would relax to form a *M*–O–*M* bridge bond.

5 Near-neighbor hetero-transition metal oxides

Unlike the example of mixed Mo-W oxide clusters, combinations of transition metals from different groups have an automatic asymmetry with respect to the metal oxidation state, and offer a greater potential for two-site cooperativity in catalysis.[143] To explore the interplay between disparate oxophilicities and stable oxidation states in *sub*oxide cluster models, we studied the structural evolution of mixed group 5-6 and 6-7 oxides, with Mo serving as the group 6 metal center in all cases. These two different

combinations offer a striking contrast between the highly oxophilic group 5 centers of V[144] and Nb,[145] both of which favor a +5 oxidation state, and the much less oxophilic group 7 Mn center,[146] which favors the +2 oxidation state. Mo has intermediate oxophilicity when compared with the group 5 and group 7 metals.[142]

Figure 3 shows a collection of PE spectra and the cluster structures determined for $MoVO_y^-$ and $MoNbO_y^-$ (y = 2–5) and $MnMoO_y^-$ (y = 3, 4). The spectra of several of the $MoVO_y^-$ clusters exhibited contributions from several structures, both of which are included in Fig. 3, verified by hole-burning PE spectroscopy.[144] Overall, these structures show the Mo center in an equal or higher oxidation state than V. This result was *surprising* based on the higher oxophilicity of V[142] and the relative *M*-O bond dissociation energies (V-O bond dissociation is 6.5 eV; Mo-O bond dissociation energy is 5.4 eV),[147] but is in line with the general trend of reducibility decreasing for elements lower on the periodic table. The structures of the second-row adjacent neighbor Mo-Nb oxides show Nb in a higher oxidation state than Mo, except in the case of $MoNbO_4^-$, which is consistent with the relative oxophilicities and M–O bond dissociation energies (Nb-O bond dissociation energy is 8.0 eV).[148] The higher electronegativity of Mo relative to Nb[148] also results in the Nb center having a more positive charge in structures with both centers nominally in the same oxidation state.

The preferential oxidation of one particular metal center in a heterometallic cluster, in which both metal centers have high, if not equal, oxophilicity suggests that in nanoscale, highly defective surfaces, a dopant metal atom will remain an electron rich (or poor) center over a range of partial oxidation of the system.

In contrast, for systems with both different oxophilicities and disparate oxidation states, such as in the case of Mn and Mo, the description of bonding in the cluster is different. Bulk $MnMoO_4$ has been explored as a catalyst for HER.[149–152] Our studies on the electronic structure and reactivity of cluster systems gave some insight into why this combination might be effective.

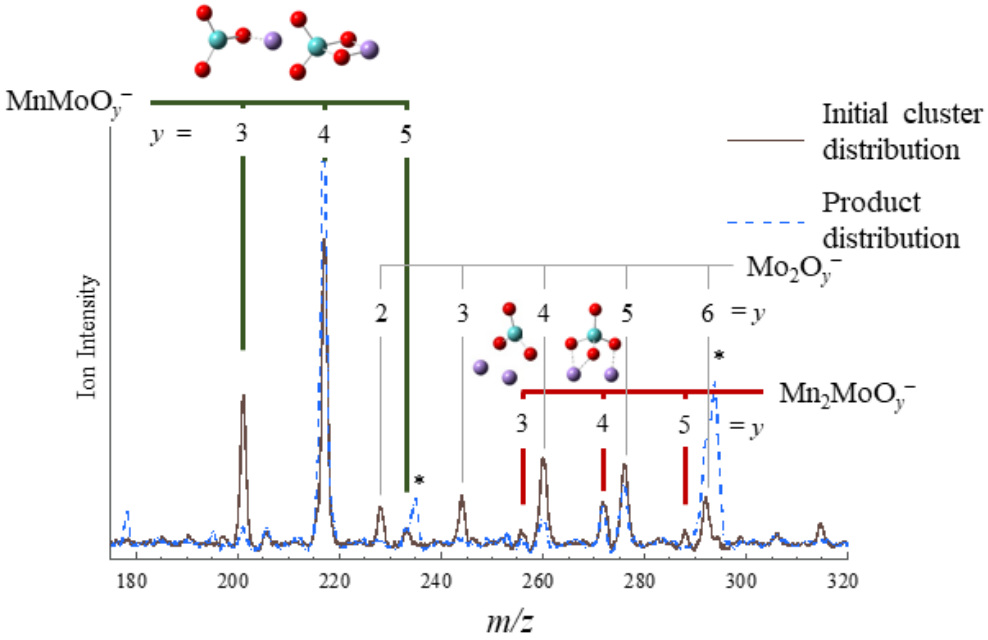

Figure 4. Initial mass distribution of clusters formed from laser ablation of a mixed ^{98}Mo/Mn target, showing Mn^{98}MoO$_y^-$ (y = 3, 4), ^{98}Mo$_2$O$_y^-$(y = 2 – 6) and Mn$_2$^{98}MoO$_y^-$ (y = 3 – 5) clusters (black trace) and distribution after reactions with water (blue dashed trace) along with the structures determined computationally. Species indicated with an asterisk (*) are water addition products. Turquoise represents Mo, rose represents Mn, red represents O.

As suggested from Figure 3 and shown explicitly in Figure 4, Mo-Mn mixed oxides did not span the broad range of oxidation states observed for the homo- and heterometallic group 6 and mixed group 5/group 6 clusters, which showed oxidation states of $2 \le y \le .3x$ where x is the total number of metal centers. Rather, the MnMoO$_y^-$ series was confined to y = 3, 4, and Mn$_2$MoO$_y^-$ to y = 3–5. In addition, both MnMoO$_3^-$ and Mn$_2$MoO$_3^-$ were oxidized by water, forming MnMoO$_4^-$ and Mn$_2$MoO$_4^-$ (releasing H$_2$) while the tetroxides underwent water addition, which does not change the overall oxidation state of the cluster.

From the PE spectra and computational results, these clusters can be described as ionic complexes. For example, MnMoO$_3^-$ and MnMoO$_4^-$ can be described as Mn$^+$·(MoO$_3$)$^{2-}$ and Mn$^+$·(MoO$_4$)$^{2-}$, while the structurally corresponding neutral are Mn^{2+}·(MoO$_3$)$^{2-}$ and Mn^{2+}·(MoO$_4$)$^{2-}$. The Mn$_2$MoO$_y^-$ (y = 3,4) clusters can be described similarly, with the positive charge shared by the Mn centers. In this picture, the particular

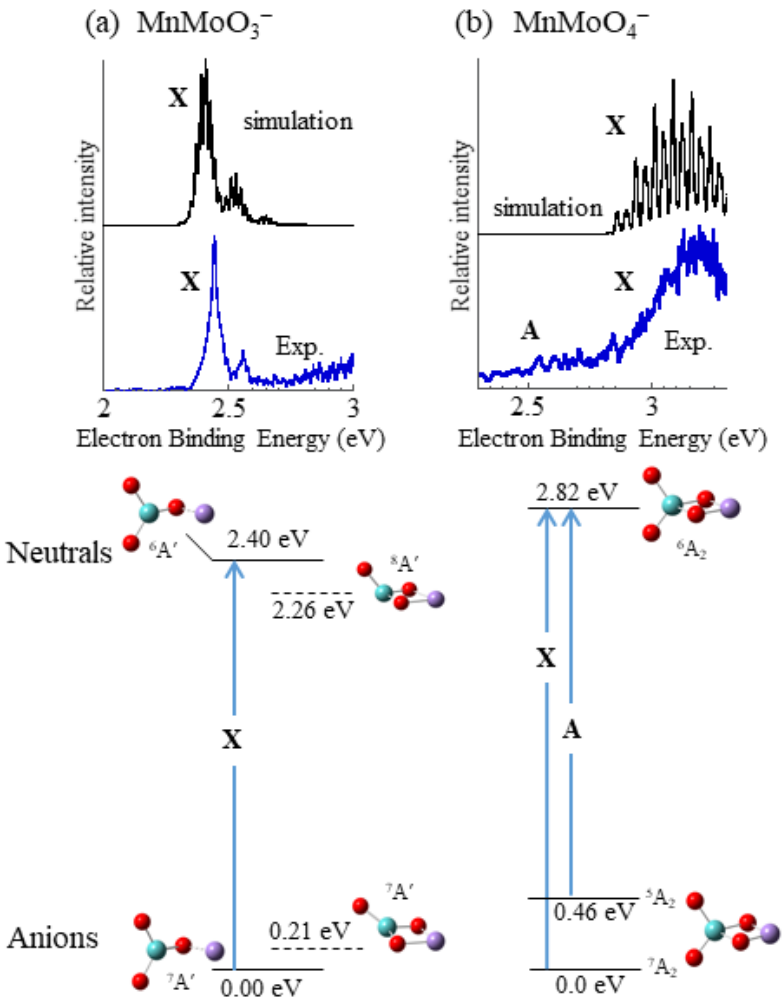

Figure 5. Spectral simulations (top frames) based on B3LYP-D3BJ computed structures for (a) $MnMoO_3$ and (b) $MnMoO_4$ anions and neutrals. Dashed lines indicate an isomer that is predicted to be energetically competitive but not observed in the spectrum. Note that when $MnMoO_4^-$ ion signal is augmented by oxidation of $MnMoO_3^-$ by water, band A becomes relatively more intense, suggesting production of electronically excited $MnMoO_4^-$.

stability of the +2 oxidation state for Mn combined with the dual stability of the +4 and +6 oxidation states of Mo create a very specifically favored distribution of clusters. The oxidation of $MnMoO_3^-$ by water toggles the oxidation state ONLY of the Mo center, from +4 to +6, leaving the Mn center in its low oxidation state. This particular result is exciting: One of the enduring challenges of using cluster models for catalysts is the irreversibly reactivity of clusters. While they still provide valuable insight into the local electronic and structural environment that support catalytic activity, modeling full-cycle processes is more elusive. In

the case of the mixed Mn-Mo oxide clusters, regeneration of the $Mn_xMoO_3^-$ chemically active cluster is feasible because of the relative stability of Mo(IV). Figure 5 shows the calculation-based simulations of (a) $MnMoO_3^-$ and (b) $MnMoO_4^-$. As seen previously, the lowest energy structure of $MnMoO_3$ is different from $MnMoO_3^-$, and the observed spectrum is consistent with the transition from the lowest energy anion to the less stable neutral structure. Also of note is the experimental spectrum of $MnMoO_4^-$, which is included in panel (b) appears to have two broad transitions separated by approximately 0.5 eV, which is consistent with the septet-quintet splitting in the precursor anion. Interestingly, the lower energy transition is enhanced when the production of $MnMoO_4^-$ was augmented by $MnMoO_3^-$ + H_2O reactions, suggesting that $MnMoO_4^-$ is produced in an excited electronic state, further supporting the idea of facile regeneration. Finally, we comment on the high spin localized on Mn^{2+} in both clusters, suggesting Mn-doped MoO_3 materials might have interesting magnetic properties.

6 Cluster models of supported catalysts: $Pt_nCe_xO_y^-$

Reports on studies of ceria-supported Pt nanoparticles having enhanced activity toward the water-gas shift reaction ($CO + H_2O \rightarrow CO_2 + H_2$)[153] along with theoretical studies highlighting the non-innocence of cerium oxide as a catalyst support material[154] motivated our cluster model studies on bare cerium oxides and mixed platinum-cerium oxide. In this case, small cluster models may be particularly appropriate, based on reports of the activity of CeO_2 nanoparticle-supported Pt-*atoms*.[155] What combination of attributes of ceria and platinum leads to enhanced activity?

Our earlier studies on $Ce_xO_y^-$ + H_2O reactions revealed a more complex reaction landscape than what was seen in the transition metal oxide reactions with water.[156,157] The most profoundly reduced clusters ($y < x$) underwent direct oxidation with H_2 production. However, the intermediate suboxide clusters underwent monohydroxide formation alongside water addition, with direct oxidation re-emerging as the clusters approached $Ce_xO_{2x}^-$ stoichometry. However, loss of ion signal under reactive conditions also suggested that chemifragmentation or chemi-detachment (i.e., chemi-ionization of the anion) might have contributed to the production or depletion of ions.

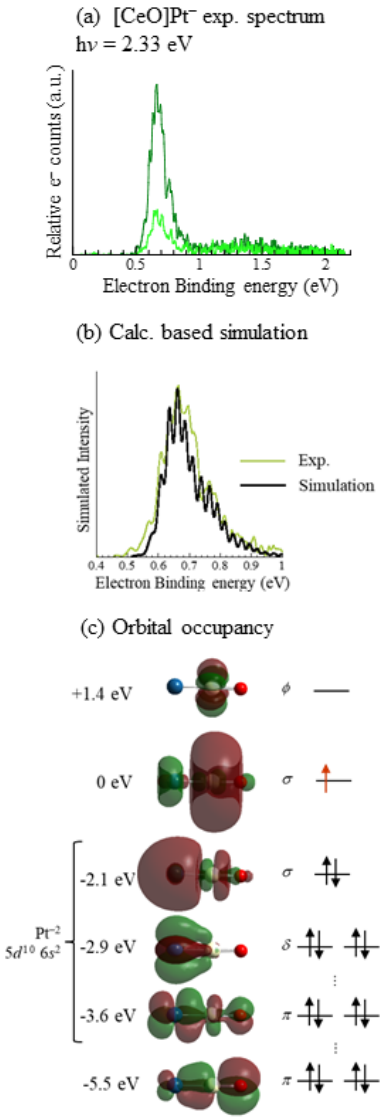

Figure 6. (a) PE spectrum of $[CeO]Pt^-$ measured using 2.330 eV photon energy, and (b) simulation based on the B3LYP-calculated linear Pt-O-Ce structure with (c) orbital occupancy shown. Orbital energies are relative to the highest singly occupied molecular orbital. Note that the Pt nominally carries a -2 charge state. Dark blue represents Pt, cream represents Ce, red represents O.

Based on the anion PE spectra and computational results, the electronic structures of $Ce_xO_y^-$ clusters are very evocative of the bulk sesquioxide electronic structure.[158] The 4f subshell in every Ce center is singly occupied for all species with $x > 2y$, with the clusters' 4f orbitals lying in a very narrow energy window between the bonding Ce 5d-O 2p orbitals (correlating to the bulk valence band), with the remaining electrons lying in diffuse, outer-valence and non-bonding 6s-based molecular orbitals, skimming

the surface of the clusters. Of relevance to the question of Pt-Ce_xO_y interactions, these electrons are weakly bound, typically by *ca.* 1 eV.

The heterometallic platinum-cerium oxides have electronic structures that are somewhat different from the near-neighbor heterometallic transition metal oxides. An early indicator was the observation of Pt^- photodetachment signal in the PE spectra of several of the complexes, signaling photodissociation followed by photodetachment of the Pt^- daughter ion at modest photon energies,[159] and suggesting relatively weak bonding compared to the other heterometallic species. An exception was the simplest cluster system, $[CeO]Pt^-$, the PE spectrum of which is shown in Figure 6(a). The structure consistent with the observed spectrum is shown, along with depictions of the molecular orbitals and the calculations-based simulation [Figure 6(b)]. Calculations on this molecule were problematic: A bent structure was predicted to be lowest in energy, but was inconsistent with the spectrum in terms of electron affinity, detachment cross section and Franck-Condon profile. The linear structure calculated to lie higher in energy was consistent with the spectrum. Based on the orbital occupancies [Figure 6(c)] the anion was aptly be described as $[CeO]^+ \cdot Pt^{2-}$, and the lowest energy neutral state as $[CeO]^{2+} \cdot Pt^{2-}$. Similar highly ionic character was inferred in the spectra and calculations on larger suboxide systems.

The calculated structure of the simplest anionic model system with bulk stoichiometry, $[CeO_2]Pt^-$, is shown in Figure 7. The orbitals are predominantly Pt-local or CeO_2-local, and the Pt−Ce internuclear distance is predicted to be 3.05 Å, suggesting that charge-dipole interactions bind the Pt^- atomic anion to neutral CeO_2. As seen in the resulting PE spectrum, broad direct detachment signal above 3 eV is accompanied by pronounced Pt^- photodetachment signal, suggesting photodissociation of a portion of the complexes to $CeO_2 + Pt^-$, as noted above. The broad direct detachment signal is due to the significant structural rearrangement upon detachment: The optimized neutral structure has a Pt-O-Ce bridge bond with orbital overlap between the bridging O-atom and 5*d* orbitals localized on the Pt center. Interestingly, this structural change is evocative of structures determined in calculations on Pt/Ce_6O_{12} clusters, which show charge transfer from Pt to the ceria cluster,[160] in striking contrast to the distinct accumulation of charge by

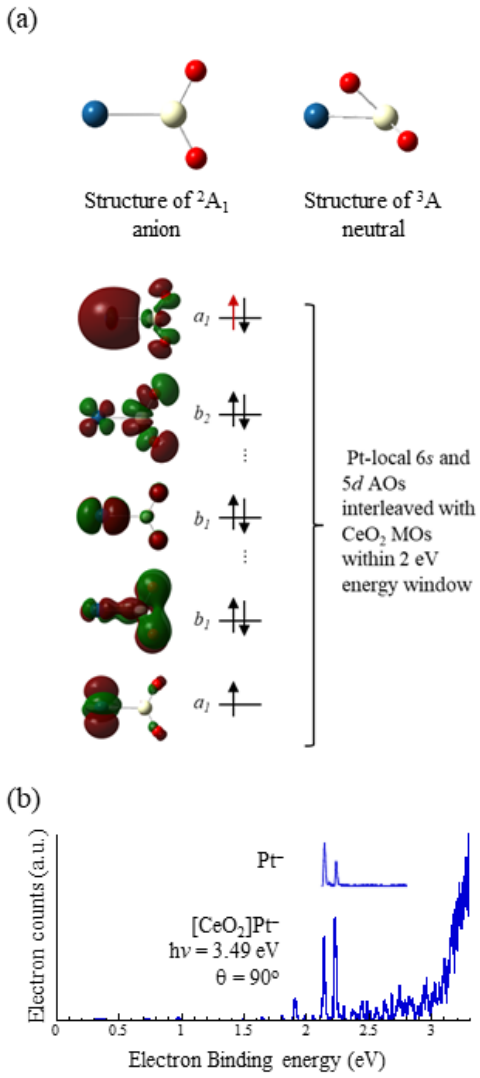

Figure 7. (a) Calculated structures of $[CeO_2]Pt$ anion and neutrals, along with orbital occupancy. The one-electron difference between the anion and neutral is indicated by the 'red' electron. The 5d orbital localize in Pt is singly occupied in both charge states. (b) PE spectrum of $[CeO_2]Pt^-$, exhibition signal due to Pt^- detachment (inset shows bare Pt^- spectrum). Direct detachment signal appears above 3 eV.

Pt in the anion. The reversal of charge transfer with the change in bonding motif driven by detachment will impact the interaction between this model active site and water-gas shift reactants.

The significant difference between the anion and neutral structures is a recurring theme in these cluster studies, and suggests the introduction of significant structural strain to an active site upon charge transfer from the catalyst (whether an active site such as an O-vacancy, or supported Pt atom).

Based on the sum of our studies, the following picture of the CeO_2/Pt_n catalyzed water-gas shift reaction emerged: Pt atoms or clusters accumulate negative charge from cerium suboxides (i.e., oxygen vacancies). Water readily reacts with cerium oxide, forming surface hydroxyl groups that are attracted to and subsequently reduced by the negatively charged Pt_n. Ceria, a material well known for its ionic conductivity (O^{2-} as the charge carrier)[161] can transport the nascent oxide to complete the oxidation of CO, which readily adsorbs on Pt.

Overall, the PE spectra and calculations supported the following: Both the electron affinities and ionization energies of cerium suboxide clusters are low, while the electron affinity of Pt is robust (2.128 eV),[162] a combination that results in particularly facile accumulation of electrons in cerium oxide-supported Pt atoms or clusters. Accumulation of negative charge by metal clusters from O-vacancies on metal oxide supports is a commonly accepted mechanism for catalytic activity, and in the case of ceria-supported Pt, the effect is augmented by the combination of specific characteristics of Pt and ceria.[163]

7 Conclusions

Use of cluster models of heterogeneous catalysts has led to a more detailed understanding of the molecular scale interactions that govern catalytic activity, as well as the role of features such as defect sites, dopants, or catalyst-support interactions. With a toolkit that includes anion PE spectroscopy and DFT calculations, which provide a detailed picture of the electronic and molecular structures of the clusters and water-addition products formed in reactivity studies, we have examined a range of homo- and heterometallic oxide cluster models for HER. The efforts have built an understanding of how local structure evolves with oxidation state, the role of metal hydride formation and hydroxyl fluxionality, and the bonding motifs that introduce barriers to metal-hydride formation.

Bulk properties of group 6 Mo- and W oxides, which have shown promise as photocatalysts for HER, are reflected in the suboxide structures formed, with the relative stability of the +4 oxidation state of

Mo driving asymmetric structures in unary $Mo_xO_y^-$ clusters. More strikingly for mixed $Mo_xW_xO_y^-$ clusters, the structures show preferential oxidation of W over Mo. The pronounced asymmetric oxidation found in heterometallic group 6 oxides and near-neighbor group 5/group 6 results in higher activity toward water, while group 7/group 6 oxides form very specific stoichiometries that suggest facile catalysts regeneration with HER. Mixed platinum-cerium oxides were probed as models for ceria supported Pt, a combination that is strikingly more active toward the water-gas shift reaction than unsupported Pt. Our results showing large negative charge accumulation by Pt, which, combined with the ionic conductivity of ceria, suggest a mechanism for the exceptionally high activity of this supported catalyst combination.

Underlying all of these studies is an understanding of both the molecular structures and how they play into the sterics of the catalyst-substrate interaction, and the electronic structures along with the structural changes associated with charge transfer. The combination of anion PE spectroscopy with DFT calculations is uniquely well suited to characterizing these structural and electronic features of cluster models for heterogeneous catalysts.

Conflicts of interest

There are no conflicts to declare.

Acknowledgements

We gratefully acknowledge support for this work from the Department of Energy grant No. DE-FG02-07ER15889, and the National Science Foundation Grant Nos. CHE-0718387, CHE-0350193, CHE-1265991, CHE-1460720, and CHE-9875046.

REFERENCES

[1] X. Cheng, Y. Li, L. Zheng, Y. Yan, Y. Zhang, G. Chen, S. Sun and J. Zhang, *Energy Environ. Sci.*, 2017, **10**, 2450–2458.

[2] N. Cheng, S. Stambula, D. Wang, M. N. Banis, J. Liu, A. Riese, B. Xiao, R. Li, T. -K. Sham, L. -M. Liu, G. A. Botton and X. Sun, *Nat. Commun.*, 2016, **7**, 13638.

[3] E. Kemppainen, A. Bodin, B. Sebok, T. Pedersen, B. Seger, B. Mei, D. Bai, P. C. K. Vesborg, J. Halme, O. Hansen, P. D. Lund and I. Chorkendorff, *Energy Environ. Sci.*, 2015, **8**, 2991–2999.

[4] G. -R. Xu, J. -J. Hui, T. Huang, Y. Chen and J. -M. Lee, *J. Power Sources*, 2015, **285**, 393–399.

[5] M. Li, Q. Ma, W. Zi, X. Liu, X. Zhu and S. Liu, *Science*, 2015, **1**, 1–7.

[6] A. J. Therrien, A. J. R. Hensley, M. D. Marcinkowski, R. Zhang, F. R. Lucci, B. Coughlin, A. C. Schilling, J. McEwen and E. C. H. Sykes, *Nat Catal*, 2018, **1**, 192–198.

[7] J. M. Thomas, *Phys. Chem. Chem. Phys.*, 2014, **16**, 7647–7661.

[8] J. Liu, *ACS Catal.*, 2017, **7**, 34–59.

[9] M. Flytzani-Stephanopoulos and B. C. Gates, *Annu. Rev. Chem. Biomol. Eng.*, 2012, **3**, 545–574.

[10] D. K. Böhme and H. Schwarz, *Angew. Chem. Int. Ed.*, 2005, **44**, 2336−2354.

[11] N. Dietl, X. Zhang, C. van der Linde, M. K. Beyer, M. Schlangen and H. Schwarz, *Chem. Eur. J.*, 2013, **19**, 3017−3028.

[12] L. G. Dodson, M. C. Thompson and J. M. Weber, *J. Phys. Chem. A*, 2018, **122**, 6909−6917.

[13] L. G. Dodson, M. C. Thompson and J. M. Weber, *J. Phys. Chem. A*, 2018, **122**, 2983−2991.

[14] M. C. Thompson, J. Ramsay and J. M. Weber, *J. Phys. Chem. A*, 2017, **121**, 7534−7542.

[15] E. Barwa, T. F. Pascher, M. Oncak, C. van der Linde and M. K. Beyer, *Angew. Chem. Int. Ed.*, 2020, **59**, 7467–7471

[16] T. F. Pascher, E. Barwa, C. van der Linde, M. K. Beyer and M. Oncak, *Theor. Chem. Acc.*, 2020, **139**, 127.

[17] J. H. Marks, T. B. Ward and M. A. Duncan, *Int. J. Mass Spec.*, 2019, **435**, 107−113.

[18] T. B. Ward, A. D. Brathwaite and M. A. Duncan, *Topics in Catal.*, 2018, **61**, 49−61.

[19] A. E. Green, S. Schaller, G. Meizyte, B. J. Rhodes, S. P. Kealy, A. S. Gentleman, W. Schollkopf, A. Fielicke and S. R. Mackenzie, *J. Phys. Chem.* A, 2020, **124**, 5389−5401.

[20] G. Meizyte, A. E. Green, A.S. Gentleman, S. Schaller, W. Schollkopy, A. Fielicke and S. R. Mackenzie, *Phys. Chem. Chem. Phys.*, 2020, **22**, 18606−18613.

[21] M. P. Klein, A. E. Ehrhard, J. Mohrbach, S. Dillinger and G. Niedner-Schatteburg, *Top. Catal.*, 2018, **61**, 106−118.

[22] S. Dillinger, J. Mohrbach and G. Niedner-Schatteburg, *J. Chem. Phys.*, 2017, **147**, 184305.

[23] J. Mohrbach, S. Dillinger and G. Niedner-Schatteburg, *J. Chem. Phys.*, 2017, **147**, 184304.

[24] S. Debnath, X. Song, M. R. Fagiani, M. L. Weichman, M. Gao, S. Maeda, T. Taketsugu, W. Schollkopf, A. Lyalin, D. M. Neumark and K. R. Asmis, *J. Phys. Chem. C*, 2019, **123**, 8439−8446.

[25] N. Dietl, T. Wende, K. Chen, L. Jiang, M. Schlangen, X. Zhang, K. R. Asmis and H. Schwarz, *J. Am. Chem. Soc.*, 2013, **135**, 3711–3721.

[26] S. Yin, Z. Wang and E. R. Bernstein, *J. Chem. Phys.*, 2013, **139**, 084307.

[27] G. E. Johnson, R. Mitrić, E. C. Tyo, V. Bonačić-Koutecký and A. W. Castleman, Jr., *J. Am. Chem. Soc.*, 2008, **130**, 13912–13920.

[28] G. E. Johnson, R. Mitrić, M. Nössler, E. C. Tyo, V. Bonačić-Koutecký and A.W. Castleman, Jr., *J. Am. Chem. Soc.*, 2009, **131**, 5460−5470.

[29] D. J. Xiao, E. D. Bloch, J. A. Mason, W. L. Queen, M. R. Hudson, N. Planas, J. Borycz, A. L. Dzubak, P. Verma, K. Lee, F. Bonino, V. Crocella, J. Yano, S. Bordiga, D. G. Truhlar, L. Gagliardi, C. M. Brown and J. R. Long, *Nat. Chem.*, 2014, **6**, 590−595.

[30] F. Dong, S. Heinbuch, Y. Xie, J. J. Rocca and E. R. Bernstein, *J. Am. Chem. Soc.*, 2008, **130**, 1932−1943.

[31] Y. Xie, F. Dong, S. Heinbuch, J. J. Rocca and E. R. Bernstein, *J. Chem. Phys.*, 2009, **130**, 114306.

[32] S. Yin, Z. -C. Wang, E. R. Bernstein, *Phys. Chem. Chem. Phys.*, 2013, **15**, 4699−4706.

[33] E. F. Fialko, A. V. Kikhtenko, V. B. Goncharov, and K. I. Zamaraev, *J. Phys. Chem. A*, 1997, **101**, 8607−8613.

[34] D. R. Justes, R. Mitrić, N. A. Moore, V. Bonačić-Koutecký and A. W. Castleman, Jr., *J. Am. Chem. Soc.*, 2003, **125**, 6289−6299.

[35] A. W. Castleman, Jr., *J. Phys. Chem. Lett.*, 2011, **2**, 1062−1069.

[36] K. A. Zemski, D. R. Justes and A. W. Castleman, Jr., *J. Phys. Chem. A*, 2001, **105**, 10237−10245.

[37] A. W. Castleman, Jr., *Catal. Lett.*, 2011, **141**, 1243−1253.

[38] W. Xue, Z. -C. Wang, S. -G. He, Y. Xie and E. R. Bernstein, *J. Am. Chem. Soc.*, 130 (2008) 15879−15888.

[39] B. V. Reddy, F. Rasouli, M. R. Hajaligol and S. N. Khanna, *Chem. Phys. Lett.*, 2004, **384**, 242−245.

[40] B. V. Reddy and S. N. Khanna, *Phys. Rev. Lett.*, 2004, **93**, 068301.

[41] S. Feyel, D. Schröder, X. Rozanska, J. Sauer and H. Schwarz, *Angew. Chem. Int. Ed.*, 2006, **45**, 4677−4681.

[42] S. Feyel, J. Döbler, D. Schröder, J. Sauer and H. Schwarz, *Angew. Chem. Int. Ed.*, 2006, **45**, 4681−4685.

[43] Y. -X. Zhao, X. -L. Ding, Y. -P. Ma, Z. -C. Wang and S. -G. He, *Theor. Chem. Acc.*, 2010, **127**, 449−465.

[44] Z. -C. Wang, S. Yin and E. R. Bernstein, *J. Phys. Chem. A*, 2013, **117**, 2294−2301.

[45] Z. -C. Wang, S. Yin and E. R. Bernstein, *Phys. Chem. Chem. Phys.*, 2013, **15**, 10429−10434.

[46] M. M. Kappes and R. H. Staley, *J. Am. Chem. Soc.*, 1981, **103**, 1286−1287.

[47] Z. Li, Z. Fang, M. S. Kelley, B. D. Kay, R. Rousseau, Z. Dohnalek and D. A. Dixon, *J. Phys. Chem. C*, 2014, **118**, 4869−4877.

[48] Z. -C. Wang, X. -N. Wu, Y. -X. Zhao, J. -B. Ma, X. -L. Ding and S. -G. He, *Chem. Eur. J.*, 2011, **17**, 3449−3457.

[49] C. J. Mundy, J. Hutter and M. Parrinello, *J. Am. Chem. Soc.*, 2000, **122**, 4837−4838.

[50] U. Buck and C. Steinbach, *J. Phys. Chem. A*, 1998, **102**, 7333−7336.

[51] L. Bewig, U. Buck, S. Rakowsky, M. Reymann and C. Steinbach, *J. Chem. Phys. A*, 1998, **102**, 1124−1129.

[52] P. J. Roach, W. H. Woodward, A. W. Castleman Jr., A. C. Reber and S. N. Khanna, *Science*, 2009, **323**, 492−495.

[53] F. A. Akin, and C. C. Jarrold, *J. Chem. Phys.*, 2004, **120**, 8698−8706.

[54] F. A. Akin and C. C. Jarrold, *J. Chem. Phys.*, 2003, **118**, 1773−1778.

[55] U. Das, K. Raghavachari, and C. C. Jarrold, *J. Chem. Phys.*, 2005, **122**, 014313.

[56] D. M. Cox, D. J. Trevor, R. L. Whetten and A. Kaldor, *J. Phys. Chem.*, 1988, **92**, 421−429.

[57] A. C. Reber and S. N. Khanna, *J. Phys. Chem. A*, 2010, **114**, 6071−6081.

[58] H. -G. Xu, X. -N. Li, X. -Y. Kong, S. -G. He and W. -J. Zheng, *Phys. Chem. Chem. Phys.*, 2013, **15**, 17126−17133.

[59] R. S. MacTaylor, W. D. Vann and A. W. Castleman, *J. Phys. Chem.*, 1996, **100**, 5329−5333.

[60] B. C. Guo, K. P. Kerns and A. W. Castleman, *J. Phys. Chem.*, 1992, **96**, 4879−4883.

[61] G. K. Koyanagi and D. K. Bohme, *J. Phys. Chem. A*, 2001, **105**, 4259−4271.

[62] J. -B. Ma, Y. -X. Zhao, S. -G. He and X. -L. Ding, *J. Phys. Chem. A*, 2012, **116**, 2049−2054.

[63] S. Feyel, D. Schröder and H. Schwarz, *Eur. J. Inorg. Chem.*, 2008, **31**, 4961−4967.

[64] K. Koszinowski, D. Schröder and H. Schwarz, *J. Phys. Chem. A*, 2003, **107**, 4999−5006.

[65] F. Aubriet, J. -J. Gaumet, W. A. de Jong, G. S. Groenewold, A. K. Gianotto, M. E. McIlwain, M. J. Van Stipdonk and C. M. Leavitt, *J. Phys. Chem. A*, 2009, **113**, 6239−6252.

[66] E. K. Parks, B. H. Weiller, P. S. Bechthold, W. F. Hoffman, G. C. Nieman, L. G. Pobo and S. J. Riley, *J. Chem. Phys.*, 1988, **88**, 1622−1632.

[67] B. H. Weiller, P. S. Bechthold, E. K. Parks, L. G. Pobo and S. J. Riley, *J. Chem. Phys.*, 1989, **91**, 4714−4727.

[68] G. Pacchioni, *Chem. Phys. Chem.*, 2003, **4**, 1041−1047.

[69] J. O. Kafader, M. Ray, K. Raghavachari and C. C. Jarrold. *J. Chem. Phys.*, 2016, **144**, 074307.

[70] R. O. Ramabhadran, J. E. Mann, S. E. Waller, D. W. Rothgeb, C. C. Jarrold, K. Raghavachari*, J. Am. Chem. Soc.*, 2013, **135**, 17039−17051.

[71] M. Ray, S. E. Waller, A. Saha, K. Raghavachari, C. C. Jarrold, *J. Chem. Phys.*, 2014, **141**, 104310.

[72] J. A. DeVine, M. C. Babin and D. M. Neumark, *Faraday Discuss*., 2019, **217**, 235−255.

[73] J. A. DeVine, A. Abou Taka, M. C. Babin, M. L. Weichman, H. P. Hratchian and D. M. Neumark, *J. Chem. Phys.*, 2018, **148**, 222810.

[74] G. Liu, P. Poths, X. Zhang, Z. Zhu, M. Marshall, M. Blankenhorn, A. N. Alexandrova, and K. H. Bowen, *J. Am. Chem. Soc.*, 2020, **142**, 7930−7936.

[75] G. Liu, S. M. Ciborowski, Z. Zhu, Y. Chen, X. Zhang and K. H. Bowen, *Phys. Chem. Chem. Phys.*, 2019, **21**, 10955−10960.

[76] P. H. Acioli, X. Zhang, K. H. Bowen and J. Jellinek, *J. Phys. Chem. C*, 2019, **123**, 7810−7817.

[77] S. Yin and E. R. Bernstein, *Phys. Chem. Chem. Phys.*, 2018, **20**, 367−382.

[78] Y. Zhang, S. Nyambo and D.-S. Yang, *J. Chem. Phys.*, 2018, **149**, 234301.

[79] N. Silver, Y. Zhang and D.-S. Yang, *J. Chem. Phys.*, 2020, **153**, 064304.

[80] R. J. Hudson, A. Falcinella and G. F. Metha, *Chem. Phys.*, 2016, **477**, 8−18.

[81] R. A. Hardy, A. M. Karayilan and G. F. Metha, *J. Phys. Chem. A*, 2020, **124**, 5812−5823.

[82] J. H. Marks, T. B. Ward and M. A. Duncan, *J. Phys. Chem. A,* 2018, **122**, 3383−3390.

[83] S. T. Akin, S. G. Ard, B. E. Dye, H. F. Schaefer, and M. A. Duncan, *J. Phys. Chem. A*, 2016, **120**, 2313−2319.

[84] N. S. Shuman, S. G. Ard, B. C. Sweeny, A. A. Viggiano, C. J. Owen and P. B. Armentrout, *J. Phys. Chem. A, 2020*, **124**, 3335−3346.

[85] M. Ghiassee and P. B. Armentrout, *J. Phys. Chem. A*, 2020, **124**, 2560−2572.

[86] J. Kim, R. M. Cox and P. B. Armentrout, *Phys. Chem. Chem. Phys.*, 2020, **22**, 3191−3203.

[87] M. Yamaguchi, Y.F. Zhang, S. Kudoh, K. Koyama, O.F. Lushchikova, J.M. Bakker, and F. Mafune, *J. Phys. Chem. Lett.*, 2020, **11**, 408−4412.

[88] F. Mafune, X. N. Liu, Y. F. Zhang and S. Kudoh, *J. Phys. Chem. A*, 2020, **124,** 7511−7517.

[89] T. J. Gorey, Y. Dai, S. L. Anderson, S. Lee, S. Lee, S. Seifert and R. E. Winans, *Surf. Sci*., 2020, **691**, 121485.

[90] G. Li, B. Zandkarimi, A. C. Cass, T. J. Gorey, B. J. Allen, A. N. Alexandrova and S. L. Anderson, *J. Chem. Phys.* 2020, **152**, 024702.

[91] G. Krishnan, N. Eom, R. M. Kirk, V. B. Golovko, G. F. Metha and G. G. Andersson, *J. Phys. Chem. C*, 2019, **123**, 6642−6649.

[92] R.T. Hanagan, G. Giannakakis, M. Flytzani-Stephanopoulos and E.C.H. Sykes, *Chem. Rev.* 2020, XXXX, XXX, XXX-XXX.

[93] R. Reocreux, P. L. Kress, R. Y. Hannagan, V. Cinar, M. Stamatakis and E. C. H. Sykes, *J. Phys. Chem. Lett.* 2020, **11**, 8751-8757.

[94] M. Leist, C. Kerner, L. Taghizadeh Ghoochany, S. Farsadpour, A. Fizia, J. P. Neu, F. Schon, Y. Sun, B. Oelkers, J. Lang, F. Menges, G. Niedner-Schatteburg, K. S. M. Salih and W. R. Thiel, *J. Organomet. Chem.*, 2018, **863**, 30−43.

[95] F. Doherty, H. Wang, M. Yang and B. R. Goldsmith, *Cat. Sci. Tech.*, 2020, **10**, 5772−5791.

[96] V. D. Moravec and C. C. Jarrold, *J. Chem. Phys.*, 1998, **108**, 1804−1810.

[97] J. A. Felton, M. Ray and C. C. Jarrold, *Phys. Rev. A*, 2014, **89**, 0334047.

[98] S. E. Waller, J. E. Mann and C. C. Jarrold, *J. Phys. Chem. A*, 2013, **117**, 1765−1772.

[99] D. W. Rothgeb, E. Hossain, A. T. Kuo, J. L. Troyer, C. C. Jarrold, N. J. Mayhall and K. Raghavachari, *J. Chem. Phys.*, 2009, **130**, 124314.

[100] M. J. Frisch, G. W. Trucks, H. B. Schlegel, G. E. Scuseria, M. A. Rob, J. R. Cheeseman, J. A. Montgomery Jr., T. Vreven, K. N. Kudin, J. C. Burant, J. M. Millam, S. S. Iyengar, J. Tomasi, V. Barone, B. Mennucci, M. Cossi, G. Scalmani, N. Rega, G. A. Petersson, H. Nakatsuji, M. Hada, M. Ehara, K. Toyota, R. Fukuda, J. Hasegawa, M. Ishida, T. Nakajima, Y. Honda, O. Kitao, H. Nakai, M. Klene, X. Li, J. E. Knox, H. P. Hratchian, J. B. Cross, V. Bakken, C. Adamo, J. Jaramillo, R. Gomperts, R. E. Stratmann, O. Yazyev, A. J. Austin, R. Cammi, C. Pomelli, J. W. Ochterski, P. Y. Ayala, K. Morokuma, G. A. Voth, P. Salvador, J. J. Dannenberg, V. G. Zakrzewski, S. Dapprich, A. D. Daniels, M. C. Strain, O. Farkas, D. K. Malick, A. D. Rabuck, K. Raghavachari, J. B. Foresman, J. V. Ortiz, Q. Cui, A. G. Baboul, S. Clifford, J. Cioslowski, B. B. Stefanov, G. Liu, A. Liashenko, P. Piskorz, I. Komaromi, R. L. Martin, D. J. Fox, T. Keith, M. A. Al-Laham, C. Y. Peng, A. Nanayakkara, M. Challacombe, P. M. W. Gill, B. Johnson, W. Chen, M. W. Wong, C. Gonzalez, and J. A. Pople, *Gaussian 03*, Gaussian, Inc., Wallingford, CT, 2003.

[101] M. J. Frisch, G. W. Trucks, H. B. Schlegel, G. E. Scuseria, M. A. Robb, J. R. Cheeseman, G. Scalmani, V. Barone, B. Mennucci, G. A. Petersson, H. Nakatsuji, M. Caricato, X. Li, H. P. Hratchian, A. F. Izmaylov, J. Bloino, G. Zheng, J. L. Sonnenberg, M. Hada, M. Ehara, K. Toyota, R. Fukuda, J. Hasegawa, M. Ishida, T. Nakajima,Y. Honda, O. Kitao, H. Nakai, T. Vreven, J. A. Montgomery, Jr., J. E. Peralta, F. Ogliaro, M. Bearpark, J. J. Heyd, E. Brothers, K. N. Kudin, V. N. Staroverov, R. Kobayashi, J. Normand, K. Raghavachari, A. Rendell, J. C. Burant, S. S. Iyengar, J. Tomasi, M. Cossi, N. Rega, J. M. Millam, M. Klene, J. E. Knox, J. B. Cross, V. Bakken, C. Adamo, J. Jaramillo, R. Gomperts, R. E. Stratmann, O. Yazyev, A. J. Austin, R. Cammi, C. Pomelli, J. W. Ochterski, R. L. Martin, K. Morokuma, V. G. Zakrzewski, G. A. Voth, P. Salvador, J. J. Dannenberg, S. Dapprich, A. D. Daniels, Ö. Farkas, J. B. Foresman, J. V. Ortiz, J. Cioslowski and D. J. Fox, *Gaussian 09 Revision D.01*, Gaussian, Inc., Wallingford, CT, 2009.

[102] M. J. Frisch, G. W. Trucks, H. B. Schlegel, G. E. Scuseria, M. A. Robb, J.R. Cheeseman, G. Scalmani, V. Barone, G. A. Petersson, H. Nakatsuji, X. Li, M. Caricato, A. V. Marenich, J. Bloino, B. G. Janesko, R. Gomperts, B. Mennucci, H. P. Hratchian, J. V. Ortiz, A. F. Izmaylov, J. L. Sonnenberg, Williams, F. Ding, F. Lipparini, F. Egidi, J. Goings, B. Peng, A. Petrone, T. Henderson, D. Ranasinghe, V. G. Zakrzewski, J. Gao, N. Rega, G. Zheng, W. Liang, M. Hada, M. Ehara, K. Toyota, R. Fukuda, J. Hasegawa, M. Ishida, T. Nakajima, Y. Honda, O. Kitao, H. Nakai, T. Vreven, K. Throssell, J. A. Montgomery, Jr., J. E. Peralta, F. Ogliaro, M. J. Bearpark, J. J. Heyd, E. N. Brothers, K. N. Kudin, V. N. Staroverov, T.A. Keith, R. Kobayashi, J. Normand, K. Raghavachari, A. P. Rendell, J. C. Burant, S. S. Iyengar, J. Tomasi, M. Cossi, J. M. Millam, M. Klene, C. Adamo, R. Cammi, J. W. Ochterski, R. L. Martin, K. Morokuma, O. Farkas, J. B. Foresman and D. J. Fox, *Gaussian 16*, Gaussian Inc., Wallingford, CT, 2016.

[103] A. D. Becke, *Phys. Rev. A*, 1988, **38**, 3098–3100.

[104] C. Lee, W. Yang and R. G. Parr, *Phys. Rev. B*, 1988, **37**, 785−789.

[105] A. D. Becke, *J. Chem. Phys.*, 1993, **98**, 5648−5652.

[106] D. Andrae, U. Haussermann, M. Dolg, H. Stoll and H. Preuss, *Theor. Chim. Acta*, 1990, **77**, 123.

[107] F. Jensen, *Introduction to Computational Chemistry*, Wiley, Chichester, 2nd ed., 2007.

[108] R. A. Kendall, T. H. Dunning and R. J. Harrison, *J. Chem. Phys.*, 1992, **96**, 6796−6806.

[109] J. M. L. Martin and A. Sundermann, *J. Chem. Phys.*, 2001, **114**, 3408−3420.

[110] Y. Zhao and D. G. Truhlar, *Acc. Chem. Res.*, 2008, **41**, 157−167.

[111] X. Cao and M. Dolg, *J. Chem. Phys.*, 2001, **115**, 7348−7355.

[112] T. H. Dunning, *J. Chem. Phys.*, 1989, **90**, 1007−1023.

[113] A. Schäfer, H. Horn and R. J. Ahlrichs*, J. Chem. Phys.*, 1992, **97**, 2571−2577.

[114] A. Schäfer, C. Huber and R. J. Ahlrichs, *J. Chem. Phys.*, 1994, **100**, 5829−5835.

[115] R. N. Schaugaard, J. E. Topolski, M. Ray, K Raghavachari and C. C. Jarrold, *J. Chem. Phys.* 2018, **148**, 054308.

[116] J. Geissbühler, J. Werner, S.M. de Nicolas, L. Barraud, A. Hessler-Wyser, M. Despeisse, S. Nicolay, A. Tomasi, B. Niesen, S. De Wolf and C. Ballif, *Appl. Phys. Lett.*, 2015, **107**, 081601.

[117] H. Simchi, B. E. McCandless, T. Meng, J. H. Boyle and W. N. Shafarman, *J. Appl. Phys.*, 2013, **114**, 013503.

[118] J. Bullock, A. Cuevas, T. Allen and C. Battaglia, *Appl. Phys. Lett.*, 2014, **105**, 232109.

[119] C. G. Granqvist, *Handbook of Inorganic Electrochromic Materials*, Elsevier, New York, 1995.

[120] F. P. Koffyberg, K. Dwight and A. Wold, *Solid State Commun*., 1979, **30**, 433−437.

[121] Z. Luo, R. Miao, T. D. Huan, I. M. Mosa, A. S. Poyraz, W. Zhong, J. E. Cloud, D. A. Kriz, S. Thanneeru, J. He, Y. Zhang, R. Ramprasad, and S. L. Suib, *Adv. En. Mat*., 2016, **6**, 1600528.

[122] R. S. Datta, F. Haque, M. Mohiuddin, B. J. Carey, N. Syed, A. Zavabeti, B. Zhang, H. Khan, K. J. Berean, J. Z. Ou, N. Mahmood, T. Daeneke and K. Kalantar-zadeh, *J. Mat. Chem. A*, 2017**, 5**, 24223−24231.

[123] G. Zheng, J. Wang, H. Liu, V. Murugadoss, G. Zu, H. Che, C. Lai, H. Li, T. Ding, Q. Gao and Z. Guo, *Nanoscale*, 2019, **11**, 18968−18994.

[124] D. W. Rothgeb, J. E. Mann and C. C. Jarrold, *J. Chem. Phys.*, 2010, **133**, 054305.

[125] D. W. Rothgeb, E.Hossain, J. E. Mann and C. C. Jarrold, *J. Chem. Phys.*, 2010, **132**, 064302.

[126] M. Ray, R. N. Schaugaard, J. E. Topolski, J. O. Kafader, K. Raghavachari and C. C. Jarrold, *J. Phys. Chem. A*, 2018, **122**, 41−52.

[127] R. B. Wyrwas, B. L. Yoder, J. T. Maze and C. C. Jarrold, *J. Phys. Chem. A*, 2006, **110**, 2157−2164.

[128] J. E. Topolski, A. K. Gupta, K. A. Nickson, K. Raghavachari, C. C. Jarrold, *Int. J. Mass. Spectrom.*, 2018, **434**, 193−201.

[129] B. L. Yoder, J. T. Maze, K. Raghavachari, and C. C. Jarrold, *J. Chem. Phys.*, 2005, **122**, 094313.

[130] J. E. Mann, N. J. Mayhall and C. C. Jarrold, *Chem. Phys. Lett.*, 2012, **525**−**526**, 1−12.

[131] N. J. Mayhall, D. W. Rothgeb, E. Hossain, C. C. Jarrold and K Raghavachari, *J. Chem. Phys.*, 2009, **131**, 144302.

[132] D. W. Rothgeb, E. Hossain, N. J. Mayhall, K. Raghavachari and C. C. Jarrold, *J. Chem. Phys.*, 2009, **131**, 144306.

[133] R. O. Ramabhadran, N.J. Mayhall and K. Raghavachari, *J. Phys Chem. Lett.*, 2010, **1**, 3066−3071.

[134] D. W. Rothgeb, E. Hossain, A. T. Kuo, J. L. Troyer and C. C. Jarrold, *J. Chem. Phys.*, 2009, **131**, 044310.

[135] M. Ray, A. Saha, and K. Raghavachari, *Phys. Chem. Chem. Phys.*, 2016, **18**, 25687−25692.

[136] D. G. Rothgeb, J. E. Mann, S. E. Waller and C. C. Jarrold, *J. Chem. Phys.*, 2011, **135**, 104312.

[137] A. Saha, K. Raghavachari, *J. Chem. Phys.*, 2013, **139**, 204301.

[138] J. Zhai, X. Huang, L. F. Cui, X. Li, J. Li and L. S. Wang, *J. Phys. Chem. A*, 2005, **109**, 6019−6030.

[139] S. Li and D. A. Dixon, *Catalysis by Nanoparticles*, Elsevier B.V., Amsterdam, 2013.

[140] S. Li, C. L. Guenther, M. S. Kelley and D. A. Dixon, *J. Phys. Chem. C*, 2011, **115**, 8072−8103.

[141] S. Li and D. A. Dixon, *J. Phys. Chem. A*, 2006, **110**, 6231−6244.

[142] K. P. Kepp, *Inorg. Chem.*, 2016, **55**, 9461−9470.

[143] P. Buchwalter, J. Rose and P. Braunstein, *Chem. Rev*. 2015, **115**, 28−126.

[144] J. E. Mann, D. W. Rothgeb, S. E. Waller and C. C. Jarrold, *J. Phys. Chem. A,* 2010, **114**, 11312−11321.

[145] S. E. Waller, J. E. Mann, D. W. Rothgeb and C. C. Jarrold, *J. Phys. Chem. A*, 2012, **116**, 9639−9652.

[146] J. L. Mason, A. K. Gupta, A. J. McMahon, C. N. Folluo, K. Raghavachari and C. C. Jarrold, *J. Chem. Phys.*, 2020, **152**, 054301.

[147] *CRC Handbook of Chemistry and Physics*, CRC Press, Boca Raton, 89th ed., 2008−2009.

[148] *CRC Handbook of Chemistry and Physics*, CRC Press: Boca Raton, 92nd ed., 2012.

[149] X. D. Yan, L. H. Tian, J. Murowchick and X. B. Chen, *J. Mater. Chem. A*, 2016, **4**, 3683−3688.

[150] Y. J. Cao, W. Y. Li, K. B. Xu, Y. X. Zhang, T. Ji, R. J. Zou, J. M. Yang, Z. Y. Qin and J. Q. Hu, *J. Mater. Chem. A*, 2014, **2**, 20723−20728.

[151] L. L. Wen, Y. Q. Sun, T. Zhang, Y. Bai, X. Y. Li, X. J. Lyu, W. P. Cai and Y. Li, *Nanotechnology*, 2018, **29**, 335403.

[152] H. Peelaers, M. L. Chabinyc and C. G. Van de Walle, *Chem. Mater.*, 2017, **29**, 2563−2567.

[153] A. Bruix, J. A. Rodriguez, P. J. Ramirez, S. D. Senanayake, J. Evans, J. B. Park, D. Stacchiola, P. Liu, J. Hrbek and F. Illas, *J. Am. Chem. Soc.*, 2012, **134**, 8968−8974.

[154] M. V. Ganduglia-Pirovano, *Catal. Today*, 2015, **253**, 20−32.

[155] S. H. Kye, H. S. Park, R. Zhang, H. J. Yng, K. H. Lee, H. Suh, J. G. Kim, M. G. Kim, G. S. Hwang and N. H. Hur, *J. Chem. Phys.,* 2020, **152**. 054715.

[156] J.A. Felton, M. Ray, S.E. Waller, J.O. Kafader and C.C. Jarrold, *J. Phys. Chem. A*, 2014, **118**, 9960−9969.

[157] J. E. Topolski, J. O. Kafader, M. Ray and C. C. Jarrold, *J. Mol. Spec.*, 2017, **336**, 1−11.

[158] J. O. Kafader, J. E. Topolski and C. C. Jarrold, *J. Chem. Phys.*, 2016, **145**, 154306.

[159] M. Ray, J. O. Kafader, J. E. Topolski and C. C. Jarrold, *J. Chem. Phys.*, 2016, **145**, 044317.

[160] M.S. Ozorio, K.F. Andriani and J.L.F. Da Silva, *Phys. Chem. Chem. Phys.*, 2020, **22**, 14099-1418.

[161] F. Yuan, Y. Zhang and W.J. Weber, *J. Phys. Chem. C*, 2015, **119**, 13153-13159.

[162] H. Hotop and W.C. Lineberger, *J. Chem. Phys.*, 1973, **58**, 2379-2387.

[163] E. Gross and G. A. Somorjai, *Top. Catal.*, 2013, **56**, 1049−1058.